

Monte Carlo Studies of the Ordering of the Three-Dimensional Isotropic Heisenberg Spin Glass in Magnetic Fields

Daisuke Imagawa* and Hikaru Kawamura†

Department of Earth and Space Science, Faculty of Science, Osaka University, Toyonaka, Osaka 560-0043, Japan
(November 6, 2018)

Spin and chirality orderings of the three-dimensional Heisenberg spin glass under magnetic fields are studied by large-scale equilibrium Monte Carlo simulations. It is found that the chiral-glass transition and the chiral-glass ordered state, which are essentially of the same character as their zero-field counterparts, occur under magnetic fields. The chiral-glass ordered state exhibits a one-step-like peculiar replica-symmetry breaking in the chiral sector, while it does not accompany the spin-glass order perpendicular to the applied field. Critical properties of the chiral-glass transition are different from those of the standard Ising spin glass. Magnetic phase diagram of the model is constructed, which reveals that the chiral-glass state is quite robust against magnetic fields. The chiral-glass transition line has a character of the Gabay-Toulouse line of the mean-field model, yet its physical origin being entirely different. These numerical results are discussed in light of the recently developed spin-chirality decoupling-recoupling scenario. Implication to experimental phase diagram is also discussed.

I. INTRODUCTION

In the studies of spin glasses, much effort has been devoted either experimentally or theoretically to the properties under magnetic fields. Unfortunately, our understanding of them still has remained unsatisfactory [1]. On theoretical side, most of the numerical studies have focused on the properties of the simple Ising model, especially the three-dimensional (3D) Edwards-Anderson (EA) model. While the existence of a true thermodynamic spin-glass (SG) transition has been established for this model in zero field, the question of its existence or nonexistence in magnetic fields has remained unsettled. This question is closely related to the hotly debated issue of whether the ordered state of the 3D Ising SG in zero field exhibits a replica-symmetry breaking (RSB) or not.

If one tries to understand real experimental SG ordering, one has to remember that many of real SG materials are more or less Heisenberg-like rather than Ising, in the sense that the random magnetic anisotropy is considerably weaker than the isotropic exchange interaction [1,2]. For example, in widely studied canonical spin glasses, *i.e.*, dilute metallic alloys such as AuFe, AgMn and CuMn, random magnetic anisotropy originated from the Dzyaloshinski-Moriya interaction or the dipolar interaction is often one or two magnitudes weaker than the isotropic RKKY interaction. Numerical simulations have indicated that the isotropic 3D Heisenberg SG with finite-range interaction does not exhibit the conventional SG order at finite temperature in zero field [1–8]. (However, see also Ref. [9].) Since applied fields generally tend to suppress the SG ordering, a true thermodynamic SG transition is even more unlikely under magnetic fields in case of the 3D Heisenberg SG.

Experimentally, however, a rather sharp transition-like behavior has been observed under magnetic fields in typical Heisenberg-like SG magnets, although it is not completely clear whether the observed anomaly corresponds to a true thermodynamic transition [1,10,11]. The situation is in contrast to the zero-field case where the existence of a true thermodynamic SG transition has been established experimentally [1]. Set aside the question of the strict nature of the SG “transition”, it is experimentally observed that a weak applied field suppresses the zero-field SG transition temperature rather quickly. For higher fields, the SG “transition” becomes much more robust to fields, where the “transition temperature” shows much less field dependence [1,10,11]. Such behaviors of the SG transition temperature under magnetic fields $T_g(H)$ were often interpreted in terms of the mean-field model [1,10]. Indeed, the mean-field Sherrington-Kirkpatrick (SK) model [12] with an infinite-range Heisenberg exchange interaction with weak random magnetic anisotropy exhibits a transition line similar to the experimental one [13], *i.e.*, the so-called de Almeida-Thouless (AT) line [14] $H \propto (T_g(0) - T_g(H))^{3/2}$ in weak-field regime where the anisotropy is important, and the Gabay-Toulouse (GT) line [15] $H \propto (T_g(0) - T_g(H))^{1/2}$ in strong-field regime where the anisotropy is unimportant. Nevertheless, if one notes that the true finite-temperature transition under magnetic fields, though possible in the

*E-mail:imag@spin.ess.sci.osaka-u.ac.jp

†E-mail:kawamura@ess.sci.osaka-u.ac.jp

infinite-range SK model, is unlikely to occur in a more realistic finite-range Heisenberg model, an apparent success of the mean-field model in explaining the experimental phase diagram should be taken with strong reservation. Thus, the question of the true nature of the experimentally observed SG “transition” under magnetic fields remains unsolved.

Recently, one of the present authors has proposed a scenario, the spin-chirality decoupling-recoupling scenario, aimed at explaining some of the puzzles concerning the experimentally observed SG transition [4]. In this scenario, *chirality*, which is a multispin variable representing the sense or the handedness of local noncoplanar spin structures induced by spin frustration, plays an essential role. As illustrated in Fig.1, locally noncoplanar spin structures inherent to the SG ordered state sustain two energetically degenerate “chiral” states, “right-handed” and “left-handed” states, characterized by mutually opposite signs of the “chiralities”. Here, one may define the local chirality by *three* neighboring Heisenberg spins \mathbf{S}_1 , \mathbf{S}_2 and \mathbf{S}_3 by,

$$\chi = \mathbf{S}_1 \cdot (\mathbf{S}_2 \times \mathbf{S}_3) . \quad (1)$$

This type of chirality is called “scalar chirality”, in distinction with “vector chirality” defined as a vector product of two neighboring Heisenberg spins, $\mathbf{S}_1 \times \mathbf{S}_2$ [16]. Note that the chirality defined by Eq.(1) is a pseudoscalar in the sense that it is invariant under global $SO(3)$ spin rotations but changes its sign under Z_2 spin reflections (or inversions which can be viewed as a combination of reflections and rotations).

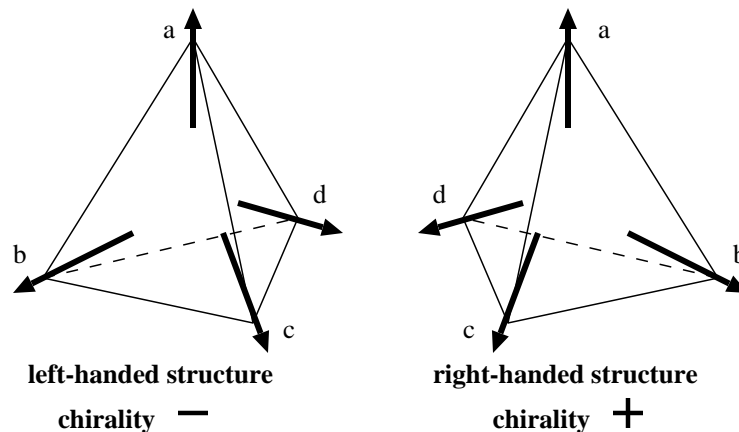


FIG. 1. Two energetically degenerate “chiral” structures characterized by the mutually opposite sign of the chirality. The labels *a-d* denote four distinct Heisenberg spins.

For a fully isotropic Heisenberg SG, in particular, the chirality scenario of Ref. [4] claims the occurrence of a novel *chiral-glass* ordered state in which only the chirality exhibits a glassy long-range order (LRO) while the spin remains paramagnetic. At the chiral-glass transition, among the global symmetries of the Hamiltonian, $O(3) = Z_2 \times SO(3)$, only the Z_2 spin reflection (inversion) symmetry is broken spontaneously with keeping the $SO(3)$ spin rotation symmetry preserved. Note that this picture entails the spin-chirality (or $SO(3) - Z_2$) decoupling on long length and time scales: Namely, although the chirality is not independent of the spin on microscopic length scale, it eventually exhibits a long-distance behavior entirely different from the spin. Such a chiral-glass transition without the conventional spin-glass order was indeed observed in recent equilibrium and off-equilibrium Monte Carlo (MC) simulations in zero field performed by Hukushima and one of the authors (H.K.) [7,8]. It was also found there that the critical properties associated with the chiral-glass transition were different from those of the Ising SG, and that the chiral-glass ordered state exhibited a one-step-like peculiar RSB.

In the chirality scenario of Ref. [4], experimental SG transition in real Heisenberg-like SG magnets is regarded essentially as a chiral-glass transition “revealed” via the random magnetic anisotropy. Weak but finite random magnetic anisotropy inherent to real magnets “recouples” the spin to the chirality, and the chiral-glass transition shows up as an experimentally observable *spin-glass* transition in real Heisenberg-like SG magnets. An interesting outcome of this picture is that the experimental SG transition is dictated by the chiral-glass transition of the fully isotropic system, *not by the spin-glass transition of the fully isotropic system*, which has been separated from the chiral one.

Very recently, the present authors discussed some of the possible consequences of the chirality scenario of Ref. [4] on the finite-field properties of the fully isotropic 3D Heisenberg SG [17]. It was argued there that the chiral-glass transition, essentially of the same character as the zero-field one, occurred also in finite fields. In the weak field regime, the transition line was predicted to behave as

$$T_{CG}(0) - T_{CG}(H) = cH^2 + dH^4 + \dots \quad , \quad (2)$$

where c and d are constants. Generally, the coefficient c could be either positive or negative. An interesting observation here is that the chiral-glass transition line (2) apparently has a form similar to the GT line of the mean-field model. We emphasize, however, that their physical origin is entirely different. The quadratic dependence of the chiral-glass transition line is simply of regular origin, whereas that of the GT-line in the SK model cannot be regarded so.

In the present paper, we report on our results of large-scale Monte Carlo simulations on the 3D isotropic Heisenberg SG, performed with the aim to reexamine the SG ordering in magnetic fields in light of the chirality scenario. In particular, by means of extensive numerical simulations, we wish to clarify in detail how the spin and the chirality order in applied fields. Part of the MC results have been reported in Ref. [17].

The present paper is organized as follows. In §II, we introduce our model and explain some of the details of our numerical method. Various physical quantities calculated in our MC simulations are defined in §III. The results of MC simulations are presented in §IV. The results for the chirality- and spin-related quantities are presented in §IV A and §IV B, respectively. It is found that the chiral-glass transition, essentially of the same character as the zero-field one, occurs under magnetic fields. The chiral-glass ordered state exhibits a one-step-like peculiar replica-symmetry breaking in the chiral sector, while it does not accompany the spin-glass order perpendicular to the applied field. Critical properties of the chiral-glass transition are analyzed in §IV C. The analysis suggests that the universality class of both the zero-field and finite-field chiral-glass transitions might be common, which, however, differs from that of the standard 3D Ising SG. In §IV D, we construct a magnetic phase diagram of the model. The chiral-glass ordered state remains quite robust against magnetic fields, while the chiral-glass transition line in applied fields has a character of the GT line of the mean-field model. Section V is devoted to summary and discussion. Our numerical results are discussed in terms of the recent experimental result on canonical SG.

II. THE MODEL AND THE METHOD

In this section, we introduce our model and explain some of the details of our numerical method. The model we consider is the isotropic classical Heisenberg model on a 3D simple cubic lattice defined by the Hamiltonian,

$$\mathcal{H} = - \sum_{\langle ij \rangle} J_{ij} \mathbf{S}_i \cdot \mathbf{S}_j - H \sum_i S_i^z, \quad (3)$$

where $\mathbf{S}_i = (S_i^x, S_i^y, S_i^z)$ is a three-component unit vector, and H is the intensity of magnetic field applied along the z direction. The nearest-neighbor coupling J_{ij} is assumed to take either the value J or $-J$ with equal probability ($\pm J$ distribution).

We perform equilibrium MC simulations on this model. Simulations are performed for a variety of fields $H/J = 0.05, 0.1, 0.5, 2.0, 3.0,$ and 5.0 , while most extensive calculations are performed for $H/J = 0.1$ and 0.5 . The lattices studied are simple-cubic lattices with $N = L^3$ sites with $L = 6, 8, 10, 12$ and 16 with periodic boundary conditions. Sample average is taken over 128-1400 independent bond realizations, depending on the system size L and the field intensity H . Limited amount of data is also taken for $L = 20$ in some cases (30 samples only) to check the size dependence of some physical quantities. To facilitate efficient thermalization, we combine the standard heat-bath method with the temperature-exchange technique [18]. Care is taken to be sure that the system is fully equilibrated. Equilibration is checked by the following procedures: First, we monitor the system to travel back and forth many times during the the temperature-exchange process (typically more than 10 times) between the maximum and minimum temperature points, and at the same time check that the relaxation due to the standard heat-bath updating is reasonably fast at the highest temperature, whose relaxation time is of order 10^2 Monte Carlo steps per spin (MCS). This guarantees that different parts of the phase space are sampled in each ‘‘cycle’’ of the temperature-exchange run. Second, we check the stability of the results against at least three times longer runs for a subset of samples. Error bars of physical quantities are estimated by the sample-to-sample statistical fluctuation over bond realizations. Further details of our Monte Carlo simulations are given in Table I.

TABLE I. Details of our MC simulations. H/J represents the magnetic-field intensity, L the lattice size, N_s the total number of samples, N_T the total number of temperature points used in the temperature-exchange run, T_{\max}/J and T_{\min}/J the maximum and minimum temperatures in the temperature-exchange run.

H/J	L	N_s	N_T	T_{\max}/J	T_{\min}/J
0.05	6	800	26	0.40	0.085
	8	600	20	0.40	0.15
	10	184	34	0.40	0.155
	12	56	34	0.40	0.155
0.1	6	1400	26	0.40	0.085
	8	1300	30	0.40	0.095
	10	1066	46	0.40	0.0975
	12	680	56	0.40	0.0975
	16	180	50	0.32	0.12
	(20)	(30)	(46)	(0.30)	(0.15)
0.5	6	800	26	0.40	0.085
	8	800	20	0.40	0.15
	10	552	34	0.40	0.155
	12	456	34	0.40	0.155
	16	128	36	0.32	0.153
	(20)	(26)	(46)	(0.30)	(0.15)
2.0	6	800	26	0.40	0.085
	8	800	20	0.40	0.15
	10	92	34	0.40	0.155
3.0	6	800	26	0.40	0.085
	8	800	20	0.40	0.15
	10	64	34	0.40	0.155
5.0	6	800	26	0.40	0.085
	8	800	20	0.40	0.15
	10	92	34	0.40	0.155

III. PHYSICAL QUANTITIES

In this section, we define various physical quantities calculated in our simulations below.

A. Chirality-related quantities

Let us begin with the definition of the chirality. We define the local chirality at the i -th site and in the μ -th direction, $\chi_{i\mu}$, for three neighboring Heisenberg spins by the scalar

$$\chi_{i\mu} = \mathbf{S}_{i+\hat{e}_\mu} \cdot (\mathbf{S}_i \times \mathbf{S}_{i-\hat{e}_\mu}), \quad (4)$$

where \hat{e}_μ ($\mu = x, y, z$) denotes a unit vector along the μ -th axis. By this definition, there are in total $3N$ local chiral variables in the system.

The mean local amplitude of the chirality, $\bar{\chi}$, may be defined by

$$\bar{\chi}^2 = \frac{1}{3N} \sum_{i=1}^N \sum_{\mu=x,y,z} [\langle \chi_{i\mu}^2 \rangle], \quad (5)$$

where $\langle \dots \rangle$ represents the thermal average and $[\dots]$ the average over the bond disorder. This quantity vanishes for coplanar spin structures, and its magnitude tells us the extent of the noncoplanarity of the local spin structures.

By considering two independent systems (“replicas”) described by the same Hamiltonian (3), one can define an overlap of the chiral variable via the relation,

$$q_\chi = \frac{1}{3N} \sum_{i=1}^N \sum_{\mu=x,y,z} \chi_{i\mu}^{(1)} \chi_{i\mu}^{(2)}, \quad (6)$$

where $\chi_{i\mu}^{(1)}$ and $\chi_{i\mu}^{(2)}$ represent the chiral variables of the replicas 1 and 2, respectively. In our simulations, we prepare the two replicas 1 and 2 by running two independent sequences of systems in parallel with different spin initial conditions and different sequences of random numbers. In terms of this chiral overlap q_χ , the chiral-glass order parameter may be defined by

$$q_\chi^{(2)} = [\langle q_\chi^2 \rangle], \quad (7)$$

while the associated chiral-glass susceptibility may be defined by

$$\chi_\chi = 3N [\langle q_\chi^2 \rangle]. \quad (8)$$

Unlike the spin variable, the local magnitude of the chirality is temperature dependent somewhat. In order to take account of this short-range order effect, we also consider the reduced chiral-glass order parameter $\tilde{q}_\chi^{(2)}$ and the reduced chiral-glass susceptibility $\tilde{\chi}_\chi$ by dividing $q_\chi^{(2)}$ and χ_χ by appropriate powers of $\bar{\chi}$,

$$\tilde{q}_\chi^{(2)} = \frac{q_\chi^{(2)}}{\bar{\chi}^4}, \quad \tilde{\chi}_\chi = \frac{\chi_\chi}{\bar{\chi}^4}. \quad (9)$$

The Binder ratio of the chirality is defined by

$$g_\chi = \frac{1}{2} \left(3 - \frac{[\langle q_\chi^4 \rangle]}{[\langle q_\chi^2 \rangle]^2} \right). \quad (10)$$

One may also define the distribution function of the chiral overlap q_χ by

$$P_\chi(q'_\chi) = [\langle \delta(q'_\chi - q_\chi) \rangle]. \quad (11)$$

In order to study the equilibrium dynamics of the model, we also compute the autocorrelation function of the chirality defined by

$$C_\chi(t) = \frac{1}{3N} \sum_{i=1}^N \sum_{\mu=x,y,z} [\langle \chi_{i\mu}(t_0) \chi_{i\mu}(t+t_0) \rangle] . \quad (12)$$

where the “time” t is measured in units of MCS. In computing (12), simulation is performed according to the standard heat-bath updating without the temperature-exchange procedure, while the starting spin configuration at $t = t_0$ is taken from the equilibrium spin configurations generated in our temperature-exchange MC runs.

We also calculate the so-called G and A parameters for the chirality, recently discussed in the literature [19–25], defined by,

$$G_\chi = \frac{[\langle q_\chi^2 \rangle^2] - [\langle q_\chi^4 \rangle]}{[\langle q_\chi^2 \rangle]^2 - [\langle q_\chi^4 \rangle]} , \quad (13)$$

$$A_\chi = \frac{[\langle q_\chi^2 \rangle^2] - [\langle q_\chi^4 \rangle]}{[\langle q_\chi^2 \rangle]^2} . \quad (14)$$

These G_χ and A_χ parameters are closely related to the sample-to-sample fluctuation of the chiral order parameter. The A parameter is known to be an indicator of the non-self-averagingness of the order parameter, *i.e.*, it vanishes in the state where the order parameter is self-averaging and takes a nonzero value otherwise [21]. By contrast, the G parameter could take a nonzero value even in a self-averaging ordered state, and hence, cannot be used as an unambiguous indicator of the non-self-averagingness [20]. However, since in the thermodynamic limit it vanishes in the high-temperature phase and takes a nonzero value in the ordered state, it can still be used as an indicator of a phase transition.

B. Spin-related quantities

As in the case of the chirality, it is convenient to define an overlap variable for the Heisenberg spin. In this case, the overlap might naturally be defined as a *tensor* variable $q_{\mu\nu}$ between the μ and ν components ($\mu, \nu=x, y, z$) of the Heisenberg spin,

$$q_{\mu\nu} = \frac{1}{N} \sum_{i=1}^N S_{i\mu}^{(1)} S_{i\nu}^{(2)} , \quad (\mu = x, y, z), \quad (15)$$

where $\mathbf{S}_i^{(1)}$ and $\mathbf{S}_i^{(2)}$ are the i -th Heisenberg spins of the replicas 1 and 2, respectively. In terms of these tensor overlaps, the “longitudinal” (parallel to the applied field) and “transverse” (perpendicular to the applied field) SG order parameters may be defined by

$$q_L^{(2)} = [\langle q_L^2 \rangle], \quad q_L^2 = q_{zz}^2, \quad (16)$$

$$q_T^{(2)} = [\langle q_T^2 \rangle], \quad q_T^2 = \sum_{\mu, \nu=x, y} q_{\mu\nu}^2 . \quad (17)$$

The associated longitudinal and transverse Binder ratios are defined by

$$g_L = \frac{1}{2} \left(3 - \frac{[\langle q_L^4 \rangle]}{[\langle q_L^2 \rangle]^2} \right), \quad (18)$$

$$g_T = \frac{1}{2} \left(6 - 4 \frac{[\langle q_T^4 \rangle]}{[\langle q_T^2 \rangle]^2} \right) . \quad (19)$$

Here, g_L and g_T are normalized so that, in the thermodynamic limit, they vanish in the high-temperature phase and gives unity in the nondegenerate ordered state.

Since an odd quantity like $\langle q_L \rangle$ does not vanish in applied fields, one can also define the “connected Binder ratio” for the longitudinal component [24],

$$g'_L = \frac{1}{2} \left(3 - \frac{[\langle (q_L - \langle q_L \rangle)^4 \rangle]}{[\langle (q_L - \langle q_L \rangle)^2 \rangle]^2} \right). \quad (20)$$

In applied fields, g'_L might well behave differently from g_L .

The spin-overlap distribution function is generally defined in the tensor space. In the following, we pay particular attention to its transverse (XY) part. The relevant transverse overlap originally has $2^2 = 4$ independent components. For the convenience of illustration, we follow Ref. [26] here and introduce the projected transverse-spin-overlap distribution function $P_T(q_{\text{diag}})$ defined in terms of the diagonal overlap q_{diag} which is the trace of the tensor overlap $q_{\mu\nu}$'s,

$$q_{\text{diag}} = \sum_{\mu=x,y} q_{\mu\mu} = \frac{1}{N} \sum_{i=1}^N (S_{ix}^{(1)} S_{ix}^{(2)} + S_{iy}^{(1)} S_{iy}^{(2)}). \quad (21)$$

The distribution function $P_T(q_{\text{diag}})$ is symmetric with respect to $q_{\text{diag}} = 0$. In the high-temperature phase, each $q_{\mu\nu}$ ($\mu, \nu = x, y$) is expected to be Gaussian-distributed around $q_{\mu\nu} = 0$ in the $L \rightarrow \infty$ limit, and so is q_{diag} .

Let us hypothesize here that there exists a transverse *spin-glass* ordered state characterized by a nonzero $q_T^{(2)}$, or by a nonzero EA transverse SG order parameter $q_T^{\text{EA}} > 0$. Reflecting the fact that q_{diag} transforms nontrivially under independent $O(2)$ rotations around the z -axis on the two replicas, which are the symmetries relevant to the transverse spin components in the presence of magnetic fields, even a self-overlap contributes nontrivial weights to $P_T(q_{\text{diag}})$ other than at $\pm q_T^{\text{EA}}$. In the $L \rightarrow \infty$ limit, the self-overlap part of $P_T(q_{\text{diag}})$ should be given by

$$P_T(q_{\text{diag}}) = \frac{1}{2} \delta(q_{\text{diag}}) + \frac{1}{2\pi} \frac{1}{\sqrt{(q_T^{\text{EA}})^2 - q_{\text{diag}}^2}}. \quad (22)$$

The derivation of Eq.(22) has been given in Ref. [26] in the context of the XY SG. If the transverse SG ordered state accompanies RSB, the associated nontrivial contribution would be added to the one given by Eq.(22). In any case, an important observation here is that, as long as the ordered state possesses a finite transverse SG LRO, the diverging peak should arise in $P_T(q_{\text{diag}})$ at $q_{\text{diag}} = \pm q_T^{\text{EA}}$ as illustrated in Fig.2, irrespective to the occurrence of the RSB.

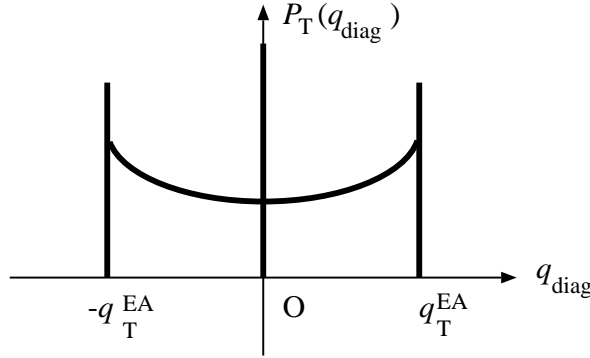


FIG. 2. Sketch of the form of the transverse diagonal-spin-overlap distribution function $P_T(q_{\text{diag}})$ in the thermodynamic limit, expected when there exists a finite transverse SG long-range order with a nonzero $q_T^{\text{EA}} > 0$.

IV. MONTE CARLO RESULTS

This section is the core part of the present paper. Here, we present our MC results on the 3D $\pm J$ Heisenberg SG in magnetic fields.

A. Chirality-related quantities

First, we begin with the chirality-related quantities. In Fig.3, we show the temperature and size dependence of the mean local amplitude of the chirality for various fields. As can clearly be seen from Fig.3(a), extrapolation of $\bar{\chi}(T)$ to $T = 0$ gives non-zero values as long as the applied field intensity is not too large, *i.e.*, $\bar{\chi}(T \rightarrow 0) \simeq 0.294, 0.295, 0.308, 0.313, 0.260,$ and 0.100 for $H/J = 0, 0.1, 0.5, 2.0, 3.0,$ and 5.0 , respectively. This indicates that the spin ordering of the 3D Heisenberg SG is certainly noncoplanar, which guarantees that the system sustains the nontrivial chirality. Meanwhile, a direct inspection of the spin pattern suggests that such noncoplanar spin configurations realized at low temperature in zero and weak fields is rather close to the coplanar one. Indeed, for completely random configurations of Heisenberg spins, $\bar{\chi}$ should take a value $\sqrt{2}/3 \simeq 0.4714 \dots$ [6], a value considerably larger than the extrapolated $\bar{\chi}(T \rightarrow 0)$ values. This again suggests that the noncoplanar configuration realized in zero and weak fields is close to the coplanar one. Interestingly, our MC data indicate that, in the weak field regime, $\bar{\chi}$ slightly *increases* with increasing magnetic field at fixed temperatures. This observation could be understood if one notes that the zero-field noncoplanar spin configuration is close to the coplanar one, and that the application of a magnetic field to such nearly coplanar spin configuration tends to “rise up” the spins from this plane with keeping the plane orthogonal to the applied field. This gives rise to more “three-dimensional” local spin structures with larger $\bar{\chi}$. Of course, when the field is further increased, $\bar{\chi}$ eventually decreases simply because strong enough fields force spins to align along the field. In Fig.3(b), we show the size dependence of $\bar{\chi}$ for the field $H/J = 0.1$. As can be seen from the figure, there is very little size dependence in $\bar{\chi}$.

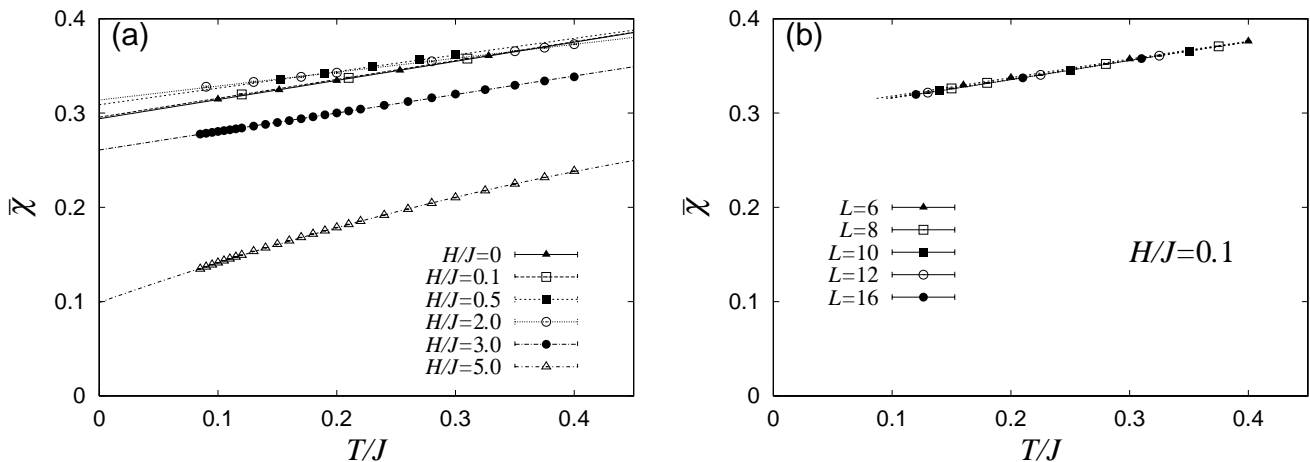


FIG. 3. Temperature dependence of the mean local amplitude of the chirality for various magnetic fields. The lattice size is $L = 16$ for $H/J = 0, 0.1$ and 0.5 , and is $L = 6$ for other field values. For the case of $H/J = 0.1$, the size dependence of $\bar{\chi}$ is shown in Fig.(b).

In Fig.4, we show the chiral-glass order parameter $q_\chi^{(2)}$ for the fields (a) $H/J = 0.1$, and (b) $H/J = 0.5$. For both fields, $q_\chi^{(2)}$ increases rather sharply at lower temperatures.

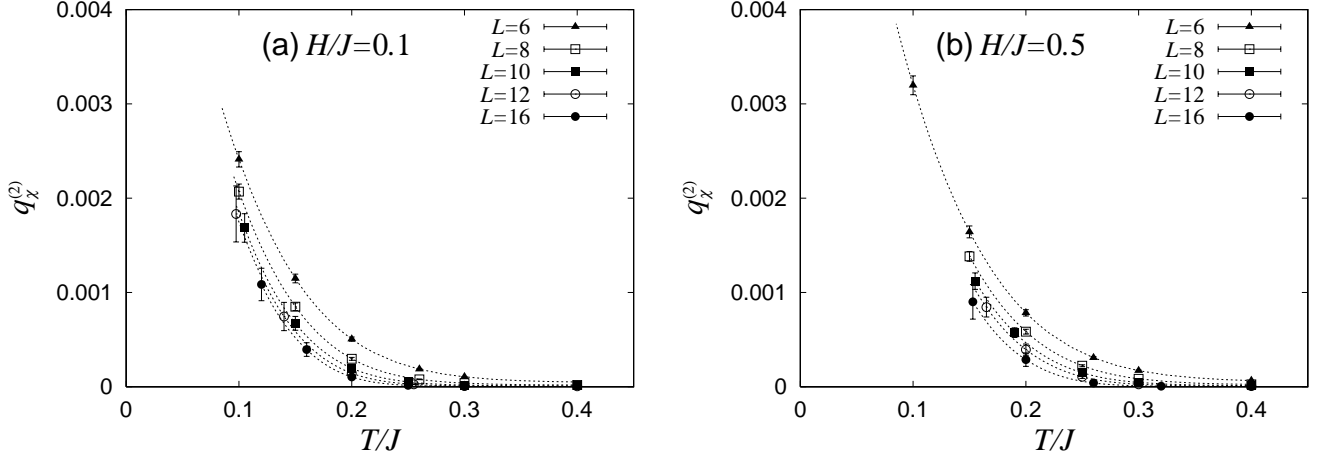


FIG. 4. Temperature and size dependence of the chiral-glass order parameter for the field (a) $H/J = 0.1$, and (b) $H/J = 0.5$.

In Figs.5(a) and (b), we show the Binder ratio of the chirality g_χ for the fields (a) $H/J = 0.1$, and (b) $H/J = 0.5$. As can be seen from the figures, g_χ exhibits a negative dip which, with increasing L , tends to deepen and shift toward lower temperature. Furthermore, g_χ of various L cross at a temperature slightly above the dip temperature T_{dip} on negative side of g_χ , eventually merging at temperatures lower than T_{dip} . The observed behavior of g_χ is similar to the one observed in zero field [8]. As argued in Ref. [8], the persistence of a negative dip and the crossing occurring at $g_\chi < 0$ are strongly suggestive of the occurrence of a finite-temperature transition where $g_\chi(T_{\text{CG}})$ takes a *negative* value in the $L \rightarrow \infty$ limit.

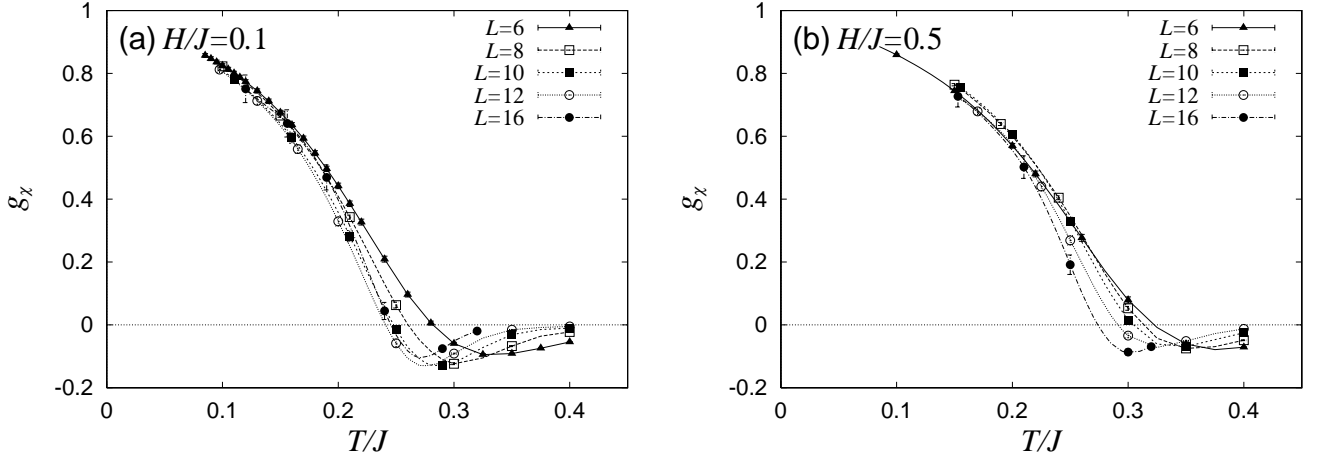


FIG. 5. Temperature and size dependence of the Binder ratio of the chirality for the fields (a) $H/J = 0.1$, and (b) $H/J = 0.5$.

In Fig.6, we plot the negative-dip temperature $T_{\text{dip}}(L)$ versus $1/L$ for the fields $H/J = 0.1$ and $H/J = 0.5$. For both fields, the data lie on a straight line fairly well. The linear extrapolation to $1/L = 0$, as shown by the solid lines in the figure, gives our first estimates of the bulk chiral-glass transition temperature, *i.e.*, $T_{\text{CG}}/J \simeq 0.23$ for $H/J = 0.1$ and $T_{\text{CG}}/J \simeq 0.25$ for $H/J = 0.5$. More precisely, $T_{\text{dip}}(L)$ should scale with $L^{-1/\nu}$ where ν is the chiral-glass correlation-length exponent. As shown below, our estimate of $\nu \simeq 1.3$ comes close to unity, more or less justifying the linear extrapolation employed here. Indeed, extrapolation with respect to $L^{-1/1.3}$, shown by the dashed curve in Fig.6, yields $T_{\text{CG}}/J \simeq 0.21$ for $H/J = 0.1$ and $T_{\text{CG}}/J \simeq 0.23$ for $H/J = 0.5$.

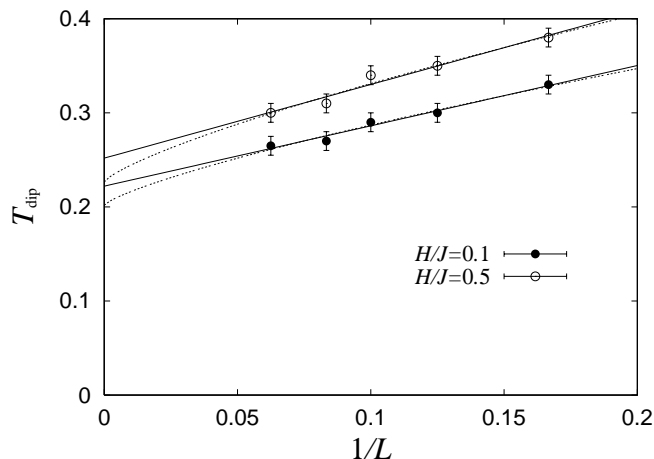


FIG. 6. The dip temperature of g_χ plotted versus $1/L$ for the fields $H/J = 0.1$ and 0.5 . $L = \infty$ extrapolation is performed, either based on the $1/L$ fit (solid line), or on the $1/L^{1.3}$ fit (dashed curve). The extrapolated values, $T_{\text{dip}}(\infty)$, give estimates of the bulk chiral-glass transition temperature T_{CG} .

As shall be argued below, we attribute several unusual features of g_χ , *e.g.*, the growing negative dip and the crossing occurring at $g_\chi < 0$, to the possible one-step-like peculiar RSB in the chiral-glass ordered state. In systems exhibiting the one-step RSB, *e.g.*, the mean-field three-state Potts glass, the Binder ratio is known to behave as illustrated in Fig.7, with a negative dip and the crossing occurring on the negative side [23]. Indeed, such a behavior is not dissimilar to the one we have observed in Fig.5.

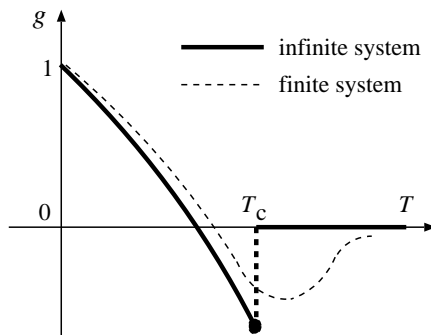


FIG. 7. Sketch of the behavior of the Binder ratio expected in a system exhibiting a one-step RSB transition. The solid curve represents the behavior of an infinite system, while the dashed curve represents that of a finite system.

An independent estimate of T_{CG} can be obtained from the equilibrium dynamics of the model. Thus, we also calculate the chirality autocorrelation function $C_\chi(t)$ defined by Eq.(12). To check the possible size dependence, we show in Fig.8 the time dependence of $C_\chi(t)$ for the field $H/J = 0.5$ on a log-log plot, computed for (a) $L = 16$, and for (b) $L = 20$. As shown in the figures, $C_\chi(t)$ shows either a downward curvature characteristic of the disordered phase, or an upward curvature characteristic of the long-range ordered phase, depending on whether the temperature is higher or lower than $T/J \simeq 0.23$. Just at $T/J \simeq 0.23$, the linear behavior corresponding to the power-law decay is observed. Hence, our data indicates that the chiral-glass transition takes place at $T_{\text{CG}}/J = 0.23(2)$, in agreement with our above estimate based on g_χ . From the slope of the data at $T = T_{\text{CG}}$, the exponent λ characterizing the power-law decay of $C_\chi(t) \approx t^{-\lambda}$ is estimated to be $\lambda = 0.13(2)$. We note that both our data of $L = 16$ shown in Fig.8(a) and of $L = 20$ shown in Fig.8(b) give almost the same estimates of T_{CG} and of λ , even though the $L = 16$ and $L = 20$ data themselves do not completely overlap, particularly below $T/J \sim 0.18$. Anyway, our observation that $C_\chi(t)$ exhibits an upward curvature below T_{CG} , tending to a nonzero value corresponding to the static chiral EA parameter $q_{\text{CG}}^{\text{EA}}$, indicates that the chiral-glass ordered state is “rigid” with a nonzero long-range order. The same analysis applied to the $H/J = 0.1$ case yields $T_{\text{CG}}/J = 0.21(2)$ and $\lambda = 0.17(2)$.

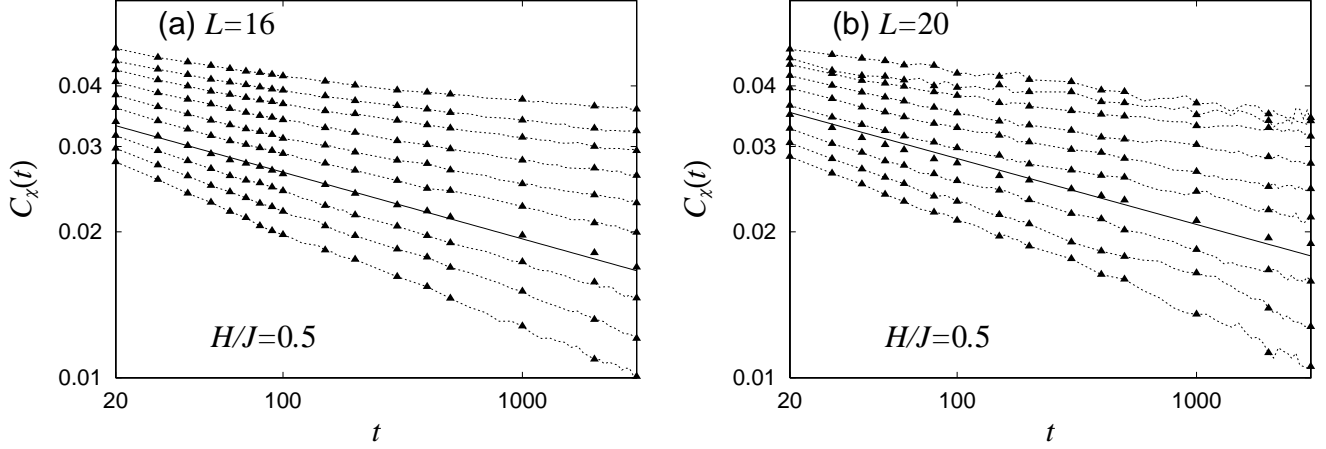


FIG. 8. Temporal decay of the equilibrium chiral autocorrelation function at various temperatures for the field $H/J = 0.5$ for the sizes (a) $L = 16$, and (b) $L = 20$. Temperatures correspond to $T/J = 0.17, 0.18, 0.19, 0.20, 0.21, 0.22, 0.23, 0.24, 0.25, 0.26$ from top to bottom. Straight lines of power-decay fit are shown in both figures (a) and (b) at $T/J = 0.23$.

In Fig.9, we show the chiral-overlap distribution function $P_\chi(q_\chi)$ for the field $H/J = 0.5$ at a temperature $T/J = 0.16$, well below T_{CG} . In addition to the standard “side-peaks” corresponding to the EA order parameter $\pm q_{CG}^{EA}$, which grow and sharpen with increasing L , there appears a “central peak” at $q_\chi = 0$ for larger L , which also grows and sharpens with increasing L . The shape of the calculated $P_\chi(q_\chi)$ is very much similar to the one obtained in Ref. [8] in zero field, but is quite different from those observed in the standard Ising-like models such as the 3D EA model [27] or the mean-field SK model [12]. As argued in Ref. [8] in case of zero field, such peculiar features of $P_\chi(q_\chi)$ are likely to be related to the *one-step*-like RSB. The existence of a negative dip in the Binder ratio g_χ and the absence of the standard type of crossing of g_χ at $g_\chi > 0$ are also consistent with the occurrence of such a one-step-like RSB [8,23]. We note that our data of $P_\chi(q_\chi)$ are also compatible with the existence of a continuous plateau between $[-q_{CG}^{EA}, q_{CG}^{EA}]$ in addition to the delta-function peaks.

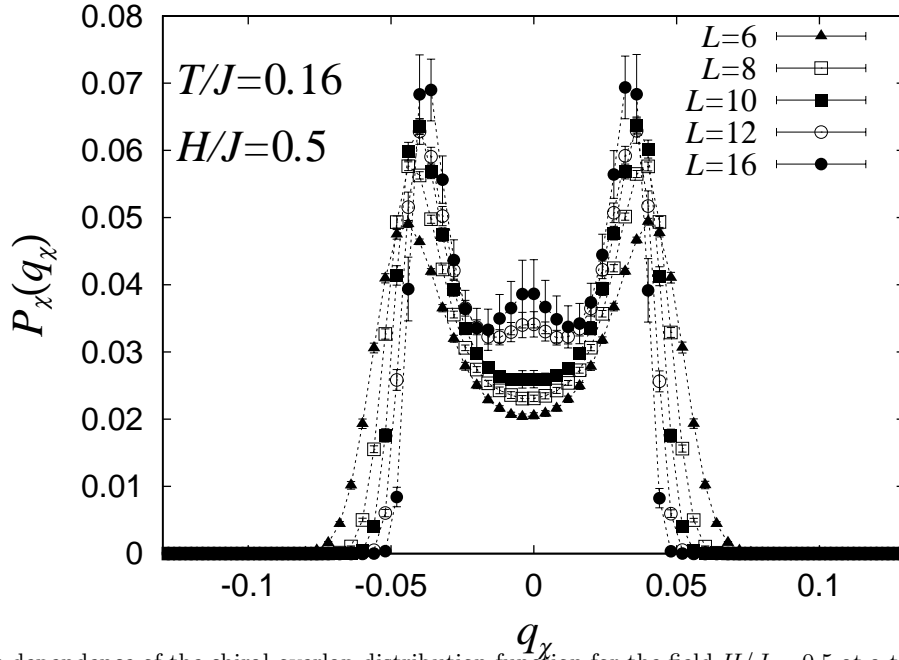


FIG. 9. The size dependence of the chiral-overlap distribution function $P_\chi(q_\chi)$ for the field $H/J = 0.5$ at a temperature $T/J = 0.16$, well below the chiral-glass transition temperature, $T_{CG}/J \simeq 0.23$.

In Fig.10, we show the the temperature and size dependence of the G_χ and A_χ parameters for the field $H/J = 0.5$.

Although error bars of the data are rather large here, the crossing occurs at temperatures somewhat higher than $T_{CG}/J \simeq 0.23$ in both figures, while the crossing temperatures of neighboring sizes (*e.g.* $L = 6$ and $L = 8$ *etc*) gradually shift towards $T_{CG}/J \simeq 0.23$ for larger L . The data are consistent with our estimate of T_{CG} above based on the Binder ratio and the autocorrelation.

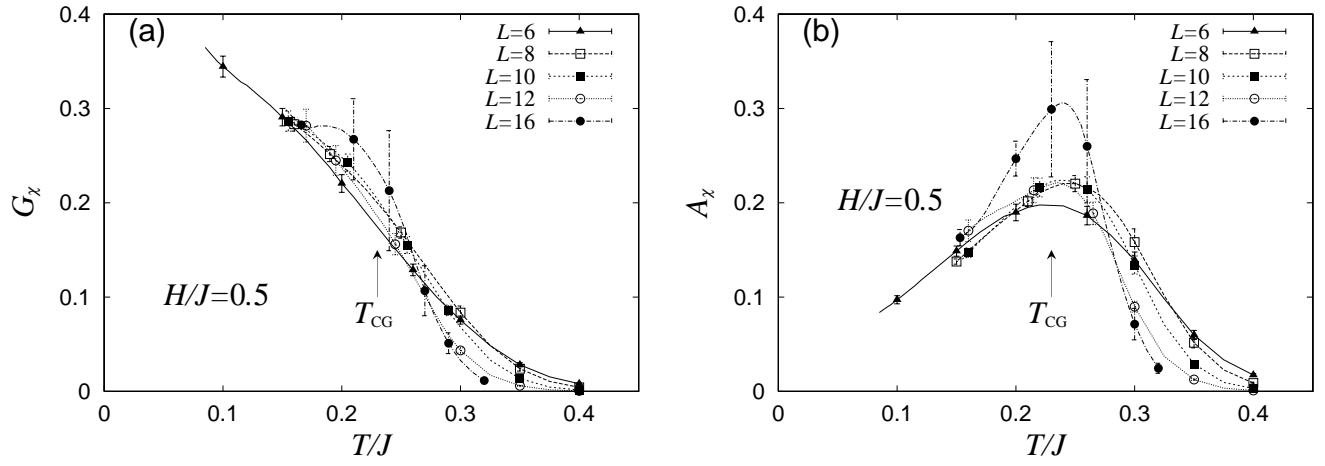


FIG. 10. Temperature and size dependence of the G and A parameters of the chirality for the field $H/J = 0.5$.

B. Spin-related quantities

In this subsection, we present our MC results of the spin-related quantities. In Figs.11 and 12, we show the spin Binder ratios for the longitudinal and transverse components, respectively, for the fields (a) $H/J = 0.1$, and (b) $H/J = 0.5$. For both fields, the *longitudinal* Binder ratio g_L increases monotonically toward unity with increasing L at all temperatures studied: See Fig.11. This observation reflects the fact that the longitudinal component of the spin exhibits a net magnetization induced by applied fields at any finite temperatures. By contrast, the Binder ratio of the transverse component of the spin g_T decreases toward zero with increasing L , without a negative dip nor a crossing: See Fig.12. This suggests that the transverse component of spin remains disordered even below T_{CG} .

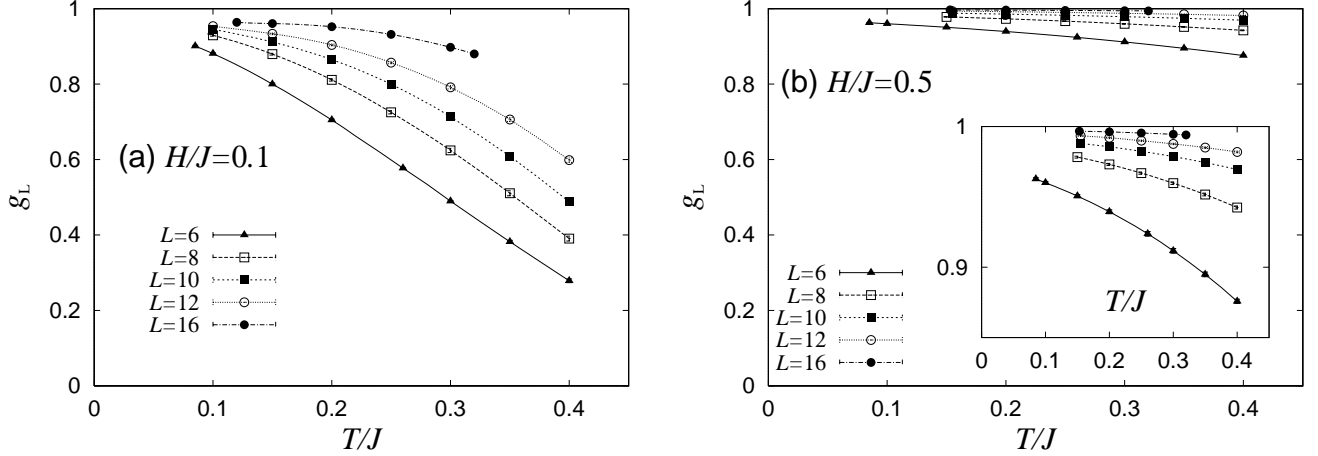


FIG. 11. Temperature and size dependence of the Binder ratio of the longitudinal-component of the spin for the fields (a) $H/J = 0.1$, and (b) $H/J = 0.5$. For the field $H/J = 0.5$, magnified figure is shown in the inset.

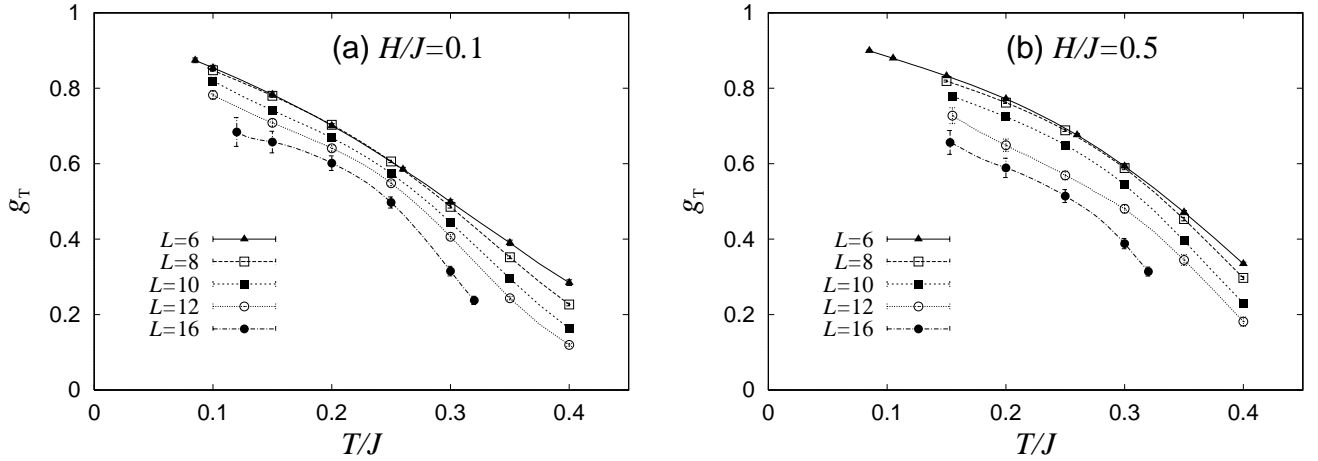


FIG. 12. Temperature and size dependence of the Binder ratio of the transverse component of the spin for the fields (a) $H/J = 0.1$, and (b) $H/J = 0.5$.

In Fig.13, we show the connected Binder ratio of the longitudinal spin component for the fields (a) $H/J = 0.1$, and (b) $H/J = 0.5$. Again, any anomalous behavior is not appreciable, no crossing nor extremum. Instead, g_L^c monotonously approaches zero with increasing L , staying negative at any temperature. (Strictly speaking, the data of $L = 6$ and $L = 8$ for $H/J = 0.1$, exhibits a crossing-like behavior around $T/J \sim 0.2$, but this is limited to these smaller lattices.)

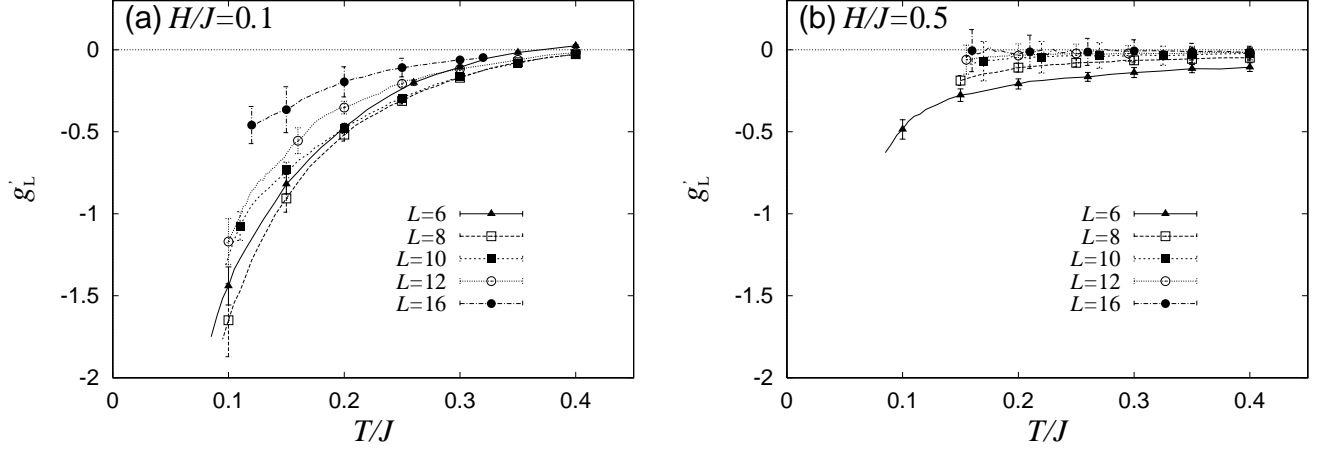


FIG. 13. Temperature and size dependence of the connected Binder ratio of the longitudinal component of the spin for the fields (a) $H/J = 0.1$, and (b) $H/J = 0.5$.

In Fig.14, we show the diagonal transverse-spin-overlap distribution function $P_T(q_{\text{diag}})$ for the field $H/J = 0.1$ at a temperature $T/J = 0.18$, well below the chiral-glass transition temperature $T_{CG} = 0.21(2)$. The calculated $P_T(q_{\text{diag}})$ exhibits a symmetric “shoulder” at some nonzero value of q_{diag} , but as shown in the inset, this “shoulder” gets suppressed with increasing L , *not showing a divergent behavior*. Such suppression of the shoulder indicates that the chiral-glass ordered state does not accompany the standard transverse SG order, at least up to temperatures $\approx (2/3)T_{CG}$. For $H/J = 0.5$, we have also observed similar suppression of the shoulder up to temperatures as low as around $\approx (2/3)T_{CG}$. Hence, we conclude that the chiral-glass ordered state does not accompany the standard transverse SG order, at least just below the chiral-glass transition point. Strictly speaking, the observed suppression of the shoulder is still not inconsistent with the Kosterlitz-Thouless(KT)-like critical SG ordered state. However, we note that such a critical SG ordered state appearing at $T \leq T_{CG}$ is not supported by our data of g_T shown in Fig.12.

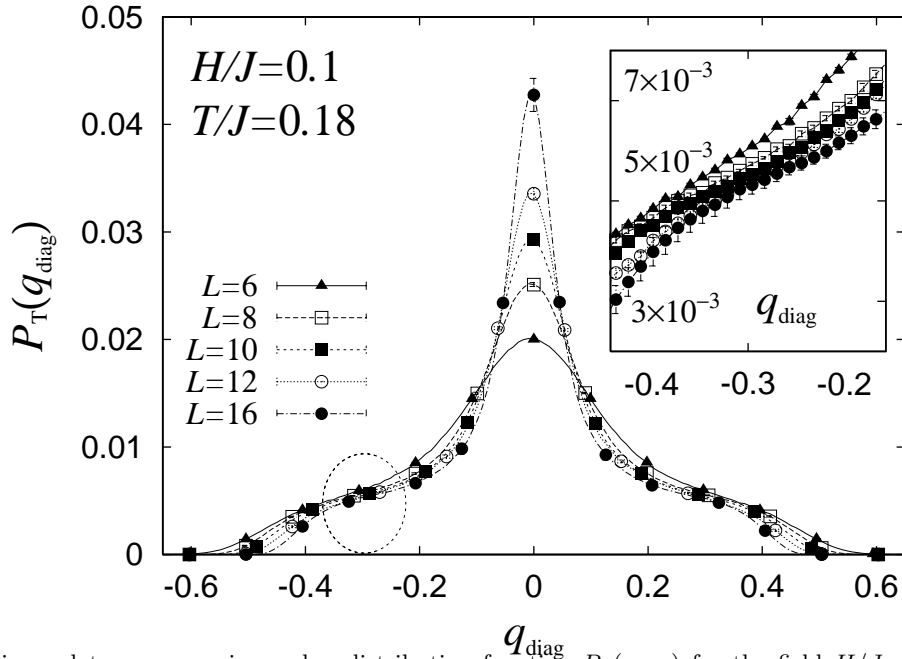


FIG. 14. The diagonal transverse-spin-overlap distribution function $P_T(q_{\text{diag}})$ for the field $H/J = 0.1$ at a temperature $T/J = 0.18$, well below the chiral-glass transition temperature $T_{CG}/J \simeq 0.21$. A magnified view of the shoulder part, indicated by the dashed circle in the main panel, is shown in the inset.

C. Critical properties of the chiral-glass transition

In this subsection, we determine static and dynamical critical exponents associated with the chiral-glass transition. The analysis here is made for the two particular field values, $H/J = 0.1$ and $H/J = 0.5$, where most extensive simulations have been performed. In the analysis below, we fix T_{CG} to be $T_{CG}/J = 0.21$ ($H/J = 0.1$) and $T_{CG}/J = 0.23$ ($H/J = 0.5$), as determined above.

We estimate first the chiral-glass susceptibility exponent γ_{CG} from the asymptotic slope of the log-log plot of the reduced chiral-glass susceptibility $\tilde{\chi}_\chi$ versus the reduced temperature $t = (T - T_{CG})/T_{CG}$. An example is given in Fig.15(a) for the case of $H/J = 0.5$, where an asymptotic slope $\gamma_{CG} = 2.0(2)$ is obtained.

We then estimate the chiral-glass critical-point-decay exponent η_{CG} from the L -dependence of the chiral-glass order parameter $\tilde{q}_\chi^{(2)}$ at T_{CG} , according to the relation $\tilde{q}_\chi^{(2)} \approx L^{-(1+\eta_{CG})}$. An example for the $H/J = 0.5$ case is shown in Fig.15(b), where we plot $\tilde{q}_\chi^{(2)}$ at $T/J = 0.23 \simeq T_{CG}/J$ versus L on a log-log plot. As can be seen from the figure, the data lie on a straight line fairly well. From its slope $\simeq 1.5$, the exponent η_{CG} is estimated to be $\eta_{CG} = 0.5(3)$.

The rest of the static exponents, α_{CG} , β_{CG} , and ν_{CG} , can be estimated from γ_{CG} and η_{CG} by using the standard scaling and hyperscaling relations as $\alpha_{CG} = -1.9(5)$, $\beta_{CG} = 0.9(4)$ and $\nu_{CG} = 1.3(3)$.

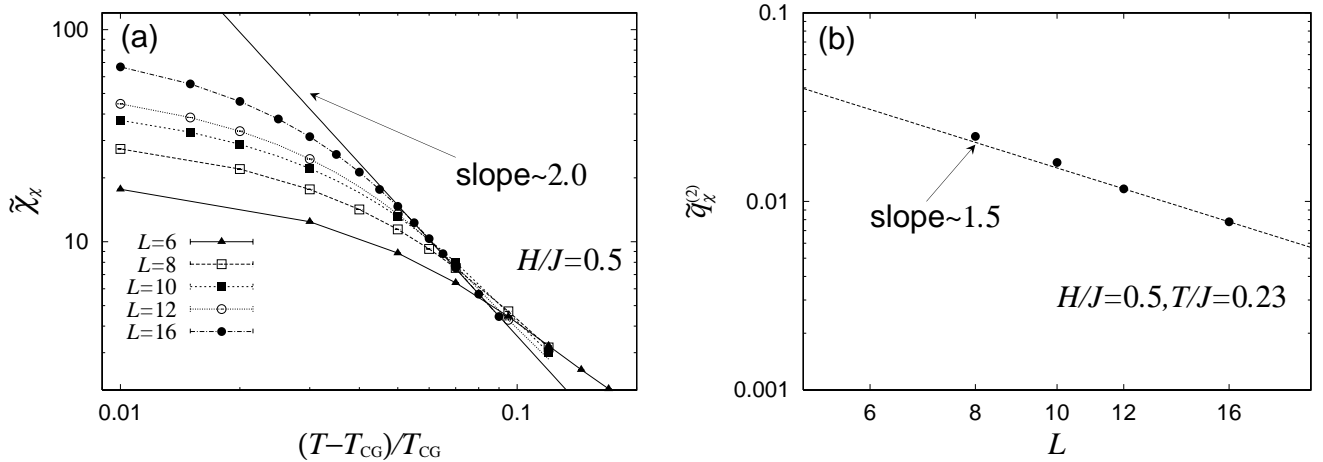


FIG. 15. (a) Log-log plot of reduced chiral-glass susceptibility $\tilde{\chi}_\chi$ versus the reduced temperature for the field $H/J = 0.5$. Its slope ≈ 2.0 determines the chiral-glass susceptibility exponent $\gamma_{CG} = 2.0(2)$. The transition temperature is assumed here to be $T_{CG}/J = 0.23$. (b) Log-log plot of $\tilde{q}_\chi^{(2)}$ versus L for the field $H/J = 0.5$ at $T/J = 0.23 \approx T_{CG}/J$. Its slope ≈ 1.5 determines the chiral-glass critical-point-decay exponent to be $\eta_{CG} = 0.5(3)$.

The dynamical exponent z_{CG} can be estimated from the exponent λ , via the relation $\lambda = \beta_{CG}/z_{CG}\nu_{CG}$. From our above estimate, $\lambda = 0.13(2)$, we get $z_{CG} = 5.3(6)$.

The same procedure is repeated for the case of $H/J = 0.1$. We then get $\nu_{CG} = 1.3(2)$, $\eta_{CG} = 0.6(3)$, $z_{CG} = 4.9(6)$. These estimates for $H/J = 0.1$ agree within errors with the corresponding estimates for $H/J = 0.5$. Our estimates of the chiral-glass exponents are summarized in Table II, and are compared with the corresponding zero-field exponents reported in Ref. [8]. The finite-field exponents turn out to agree within errors with the corresponding zero-field exponents, suggesting that the zero-field and finite-field chiral-glass transitions lie in a common universality class. We note that this observation is consistent with the chirality scenario of Refs. [4,17]. In Table II, we also show the SG exponents of the 3D Ising EA model [27,28] together with typical experimental values (in zero field) of real Heisenberg-like SG magnet AgMn [29]. The critical properties of the chiral-glass transition differ clearly from those of the 3D Ising EA SG. By contrast, the chiral-glass exponents are close to the experimental exponent values for canonical SG AgMn, giving further support to the spin-chirality decoupling-recoupling scenario.

TABLE II. List of various critical exponents for the chiral-glass transition in zero- and in finite fields, compared with the corresponding spin-glass exponents of the 3D Ising EA model [27,28] and of real Heisenberg-like SG magnet AgMn determined experimentally [29].

	α	β	γ	ν	η	z
chiral-glass: $H/J = 0.1$	~ -2.0	~ 1.0	~ 1.8	~ 1.3	~ 0.6	~ 4.9
chiral-glass: $H/J = 0.5$	~ -2.0	~ 0.9	~ 2.0	~ 1.3	~ 0.5	~ 5.3
chiral-glass: $H/J = 0^{\text{S}}$)	~ -1.7	~ 1.1	~ 1.5	~ 1.2	~ 0.8	~ 4.7
3D Ising EA ^{27,28)}	~ -1.9	0.55-0.67	4.0-4.7	1.7-2.0	-0.37--0.26	6.0-7.0
AgMn ²⁹⁾	-2.2--1.9	0.9-1.0	2.1-2.2	1.3-1.5	0.3-0.4	~ 5.4

As a consistency check of our estimates of exponents and T_{CG} values, we have also done the following: We use the ν_{CG} value determined above, $\nu_{CG} \sim 1.3$, and extrapolate the dip temperature of g_χ , $T_{dip}(L)$, to $L = \infty$ (see the dashed lines of Fig.6). As mentioned, such an extrapolation yields the bulk chiral-glass transition temperature, $T_{CG} = 0.21(2)$ ($H/J = 0.1$) and $T_{CG} = 0.23(2)$ ($H/J = 0.5$). These estimates of T_{CG} agree with those obtained from the chiral autocorrelation and employed in our scaling analysis. This guarantees that our analysis of exponents and T_{CG} is self consistent.

In Fig.16, we show the the standard finite-size scaling plot for the chiral-glass order parameter $q_\chi^{(2)}$ based on the relation,

$$q_\chi^{(2)} \approx L^{-(1+\eta_{CG})} f(Lt^{-1/\nu_{CG}}) , \quad (23)$$

where the T_{CG} , η_{CG} and ν_{CG} values are set to the best values determined above. As can be seen from the figures, reasonable data collapsing are obtained, at least for larger lattices. At the same time, however, one sees that there exists a systematic deviation from the scaling for smaller lattices, particularly in the case of $H/J = 0.1$. Such a deviation observed for smaller lattices suggests the existence of a significant finite-size correction.

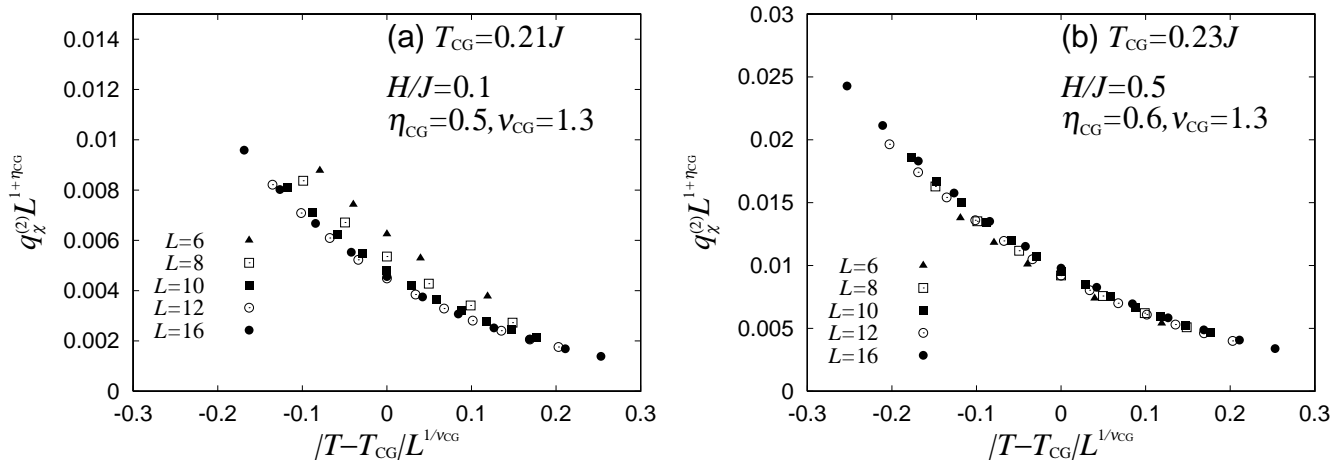


FIG. 16. Finite-size plot of the chiral-glass order parameter for the fields (a) $H/J = 0.1$, and (b) $H/J = 0.5$.

The existence of such significant finite-size effects has also been suggested from the behavior of the chiral-overlap distribution function $P_\chi(q_\chi)$ and of the chiral Binder ratio g_χ . In a truly asymptotic critical regime, $P_\chi(q_\chi)$ itself should scale at $T = T_{CG}$ with tuning one exponent η_{CG} . However, in the range of sizes studied here $L \leq 16$, we cannot observe such a full scaling of $P_\chi(q_\chi)$. Such a lack of complete scaling of $P_\chi(q_\chi)$ gives rise to certain degrees of uncertainty in our estimate of η_{CG} : Namely, if one tries to scale the width of the distribution such as its second moment $q_\chi^{(2)}$, it yields $\eta_{CG} \sim 0.5$ as given above (see Fig. 15(b)), while if one tries to scale the height of $P_\chi(q_\chi)$, it instead yields $\eta_{CG} \sim 0.4$, which is somewhat smaller than the above estimate, though still lying within the quoted error bar. Lack of a complete scaling in $P_\chi(q_\chi)$ is also reflected in the behavior of g_χ , which does not show a unique crossing at $T = T_{CG}$ within the range of sizes studied: Instead, as shown in Fig.5, the crossing occurs on the negative side of g_χ considerably above $T = T_{CG}$, while the crossing points tend to come down toward T_{CG} as L increases.

Concerning the transverse spin order, from the behaviors of the Binder ratio and of the diagonal transverse-spin-overlap distribution function, we have already found a strong numerical evidence that the chiral-glass transition does not accompany the transverse SG order, at least just below T_{CG} . In other words, the transverse component of the spin orders only at zero temperature, or else, if it orders at a finite temperature, the associated transverse SG transition temperature T_{SG} is significantly lower than T_{CG} , say, below $\approx (2/3)T_{CG}$. We warn the reader here that, so long as one looks at the SG correlation or the SG order parameter, a rather careful analysis is required to really see such a behavior. As an example, we show in Fig.17 the standard finite-size scaling plots of the transverse SG order parameter $q_T^{(2)}$ for $H/J = 0.1$; (a) the one assuming $T_{SG} = 0$, and (b) the other assuming $T_{SG} = 0.21J (= T_{CG})$. Similar plots are given in Fig.18 for the field $H/J = 0.5$ with assuming $T_{SG} = 0$, assuming (a) $T_{SG} = 0$ and (b) $T_{SG} = 0.23J (= T_{CG})$. At a look, both fits seem equally acceptable without appreciable difference if the exponents are adjusted in appropriate ways. Then, one may wonder if the transverse spin might order simultaneously with the chirality, with the associated SG exponents $\nu_{SG} \simeq 1.1 (\simeq \nu_{CG})$ and $\eta_{SG} \simeq -0.25$: See Fig.17. We believe, however, this not to be the case due to the following reasons.

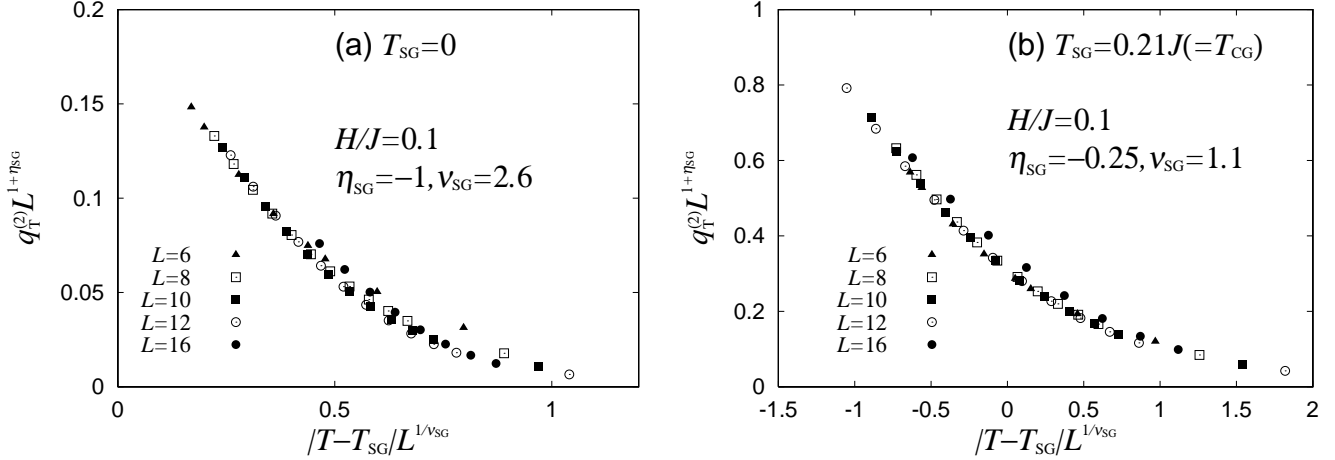


FIG. 17. Finite-size scaling plot of the transverse spin-glass order parameter for the field $H/J = 0.1$, assuming (a) $T_{SG} = 0$, and (b) $T_{SG} = 0.21J (= T_{CG})$.

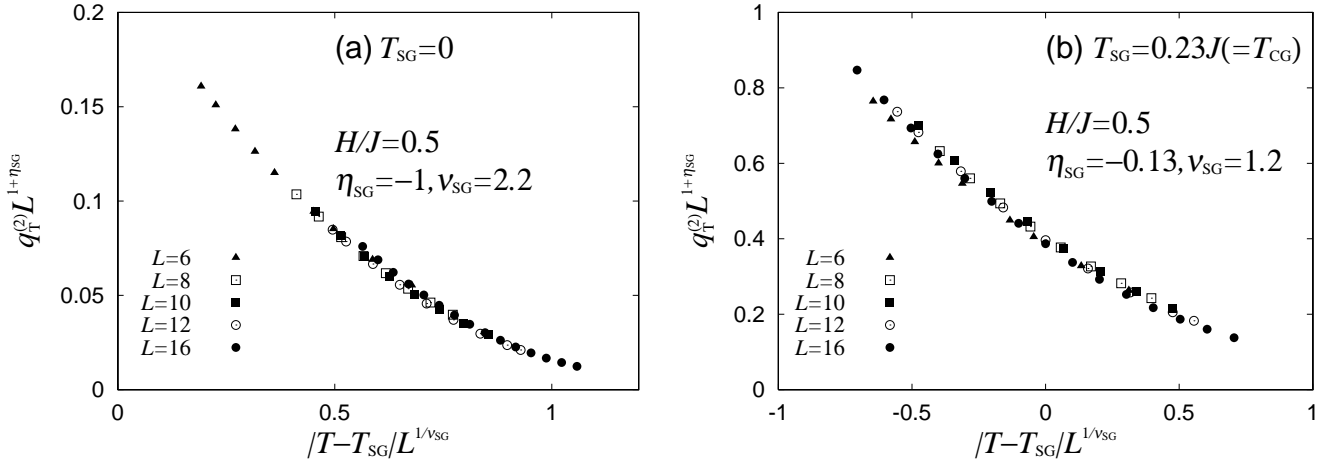


FIG. 18. Finite-size scaling plot of the transverse spin-glass order parameter for the field $H/J = 0.5$, assuming (a) $T_{SG} = 0$, and (b) $T_{SG} = 0.23J (= T_{CG})$.

First, as shown above, such simultaneous chirality and transverse-spin ordering contradicts with our result of the Binder ratio g_T and the diagonal transverse-spin-overlap distribution function $P_T(q_{\text{diag}})$. Second, a closer inspection of the data reveals that, at and below $T = T_{CG}$, there exists an important difference between the behaviors of the transverse spin $q_T^{(2)}$ and of the chirality $q_\chi^{(2)}$.

In Fig.19, we show on a log-log plot the size dependence of the both order parameters, $q_T^{(2)}$ and $q_\chi^{(2)}$, at several temperatures at and below T_{CG} . As can be seen from Fig.19(a), below T_{CG} the chiral-glass order parameter exhibits a clear upbending for larger L , indicating that $q_\chi^{(2)}$ tends to a nonzero value in the thermodynamic limit. In sharp contrast to this, such an upbending is never seen in the transverse SG order parameter $q_T^{(2)}$: Instead, $q_T^{(2)}$ shows a slight downbending behavior at $T = T_{CG}$, which gradually shifts to the near linear behavior at lower temperatures. The observed behavior of $q_T^{(2)}$ is consistent with either, (a) the onset of the Kosterlitz-Thouless(KT)-like transition at a finite temperature below which the spin-glass correlations decay algebraically with a power-law or, (b) the gradual growth of the transverse SG correlation length ξ which exceeds the investigated system size $L = 16$ around a certain nonzero temperature close to T_{CG} . In the former case, there should exist a well-defined finite SG transition temperature with the critical SG ordered state, while, in the latter case, there need not be a thermodynamic SG transition at a finite temperature. Generally speaking, it is difficult to discriminate between the above two possibilities only from the $q_T^{(2)}$ data of finite sizes with $L \leq \xi$.

Nevertheless, we believe we can at least exclude here the possibility that the KT-like transverse SG transition

occurs *simultaneously* with the chiral-glass transition at $T = T_{CG}$, accompanied by the critical SG ordered state at $T \leq T_{CG}$. First, we note that such a critical SG ordered state is not supported by our data of g_T of Fig.12. Second, the transverse *spin-glass* correlation-length exponent estimated in Figs.17(b) and 18(b) assuming the simultaneous spin and chiral transition, $\nu \simeq 1.1$, is far from the lower-critical-dimension (LCD) value, $\nu = \infty$, generically expected for such a KT-like transition. In so far as one insists that the transverse SG order occurs simultaneously with the chiral-glass order, our numerical estimate of the transverse SG correlation-length exponent is not compatible with the LCD value $\nu = \infty$, which is now hard to reconcile with the KT-like behavior observed in $q_T^{(2)}$ at $T \leq T_{CG}$.

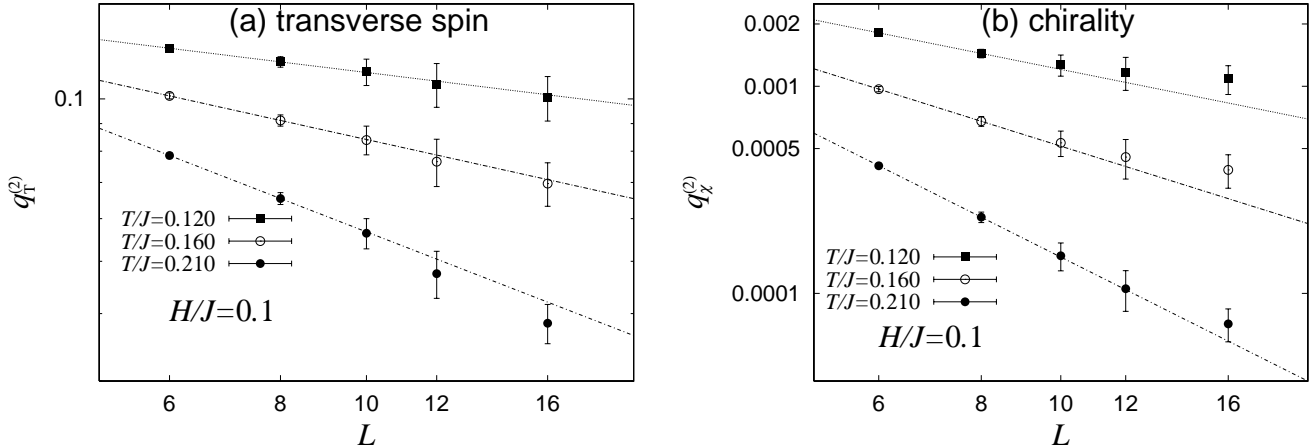


FIG. 19. Size dependence of the order parameter for the field $H/J = 0.1$, at several temperatures at and below T_{CG} : (a) the transverse-spin-glass order parameter $q_T^{(2)}$, and (b) the chiral-glass order parameter $q_\chi^{(2)}$. The chiral-glass transition temperature at this field is $T_{CG}/J \simeq 0.21$. To emphasize the deviation from the linearity, lines connecting the two small-size data $L = 6$ and 8 are drawn at each temperature.

In fact, as recently argued in Ref. [26] for the case of the *XYSG*, the chirality scenario gives the possible cause why simultaneous spin and chiral orderings are apparently observed in the SG order parameter or the SG correlation function. This would closely be related to the length and time scales of the measurements. Here, one should be aware of the fact that the spin-chirality decoupling is a *long-scale* phenomenon: At short scale, the chirality is never independent of the spin by its definition, roughly being its squared ($\chi \sim S_T^2 S_L \sim S_T^2$) as expected from the naive power counting. Hence, the behavior of the spin-correlation related quantities, including the SG order parameter which is a summed correlation, might well reflect the critical singularity associated with the *chirality* *i.e.*, the one of the chiral-glass transition, up to certain length and time scale. In such a scenario, apparent (not true) transverse “spin-glass exponents” expected would be $\nu'_{SG} \sim \nu_{CG} \sim 1.3$ and $\eta'_{SG} \sim -0.25$, the latter being derived from the short-scale relation, $1 + \eta_{CG} \sim 2(1 + \eta'_{SG})$. Note that these values are not very far from the ones we get from the finite-size scaling analysis of Figs.17(b) and 18(b), assuming the simultaneous occurrence of the spin and chiral transition. However, we stress again that such a disguised criticality in the spin sector is only a short-scale phenomenon, not a true critical one.

D. Phase diagram

By collecting our estimates of the T_{CG} values for various field values, as obtained by the extrapolation of $T_{dip}(L)$ to $L = \infty$, we construct a phase diagram in the temperature vs. magnetic field plane. The result is shown in Fig.20. We have used here the zero-field estimate of Ref. [30], $T_{CG}/J = 0.21(2)$. Error bars are estimated here from the differences between the extrapolated T_{CG} values via the $1/L$ and $1/L^{1.3}$ fits. As is evident from Fig.20, the chiral-glass state remains quite robust against magnetic fields. This is most evident in Fig.20(b) where we draw the same phase diagram on a plot where both the temperature and the magnetic-field axes have common energy scale. Indeed, $T_{CG}(H)$ is not much reduced from the zero-field value even at a field as large as ten times of $T_{CG}(0)$. At lower fields, the chiral-glass transition line is almost orthogonal to the $H = 0$ axis, consistent with the behavior Eq.(2) derived from the chirality scenario. Our data are even not inconsistent with the coefficient c in Eq.(2) being slightly negative so that $T_{CG}(H)$ initially *increases* slightly with H , though it is difficult to draw a definite conclusion due to the scatter of our estimate of $T_{CG}(H)$. If one remembers here our MC observation that the application of a weak magnetic field tends to increase

the mean local amplitude of the chirality, $\bar{\chi}$, from its zero-field value, such an initial increase of $T_{CG}(H)$ seems not totally unlikely.

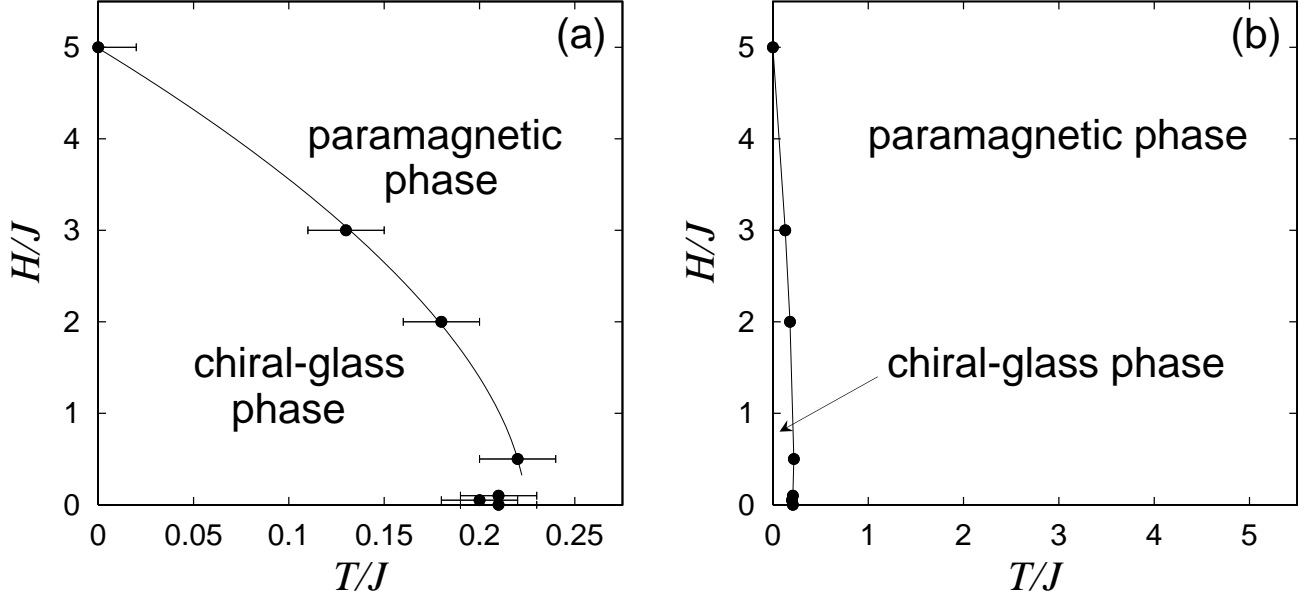


FIG. 20. $H-T$ phase diagram of the 3D $\pm J$ Heisenberg SG determined by the present simulation. Note that the energy scales of the H and of the T axes are mutually different in Fig.(a), while they are taken to be common in Fig.(b).

V. SUMMARY AND DISCUSSION

In summary, we have performed large-scale equilibrium Monte Carlo simulations on the 3D isotropic Heisenberg SG in finite magnetic fields. We have confirmed that our MC results are consistent with the chirality scenario of Ref. [4]. Among other things, we have verified the occurrence of a finite-temperature chiral-glass transition in applied fields, essentially of the same character as the zero-field one. The chiral-glass ordered state exhibits a one-step-like peculiar RSB, while it does not accompany the transverse SG order, at least up to temperatures around $\approx (2/3)T_{CG}$. The criticality of finite-field chiral-glass transitions seems to be common with that of the zero-field one, which, however, clearly differs from the criticality of the standard 3D Ising EA model. Meanwhile, the chiral-glass exponents turn out to be close to the experimental exponents determined for canonical SG such as AgMn. We have also constructed a magnetic phase diagram of the 3D Heisenberg SG model. The chiral-glass transition line in the $H-T$ plane is found to be almost vertical to the temperature axis, up to rather high fields of order $H \sim 10T_{CG}(0)$, indicating that the chiral-glass ordered state is quite robust against magnetic fields. This somewhat surprising property probably arises from the fact that the magnetic field couples in the Hamiltonian directly to the spin, *not to the chirality*, and the effective coupling between the field and the chirality is rather weak. The chiral-glass transition line has a character of the Gabay-Toulouse line of the mean-field model, yet its physical origin being entirely different.

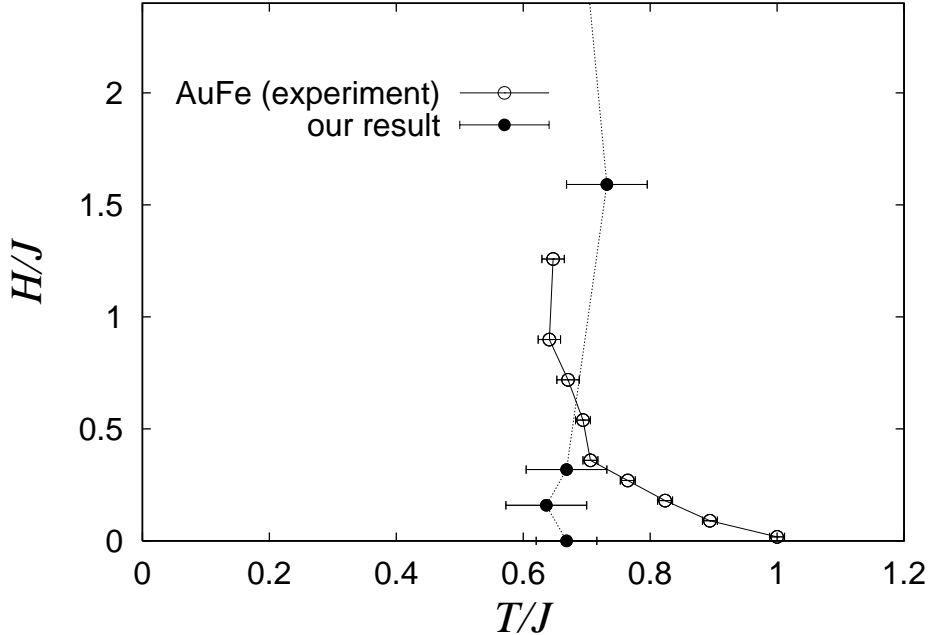


FIG. 21. Experimental phase diagram of AuFe as determined by Campbell *et al* by means of torque measurements [Ref. [11]]. For comparison, we also show the present numerical result of the magnetic phase diagram of the 3D $\pm J$ Heisenberg SG model. The way how we scale the units of magnetic field and temperature in plotting the experimental data is explained in the text.

It is not immediately possible to make a direct comparison of our results with experiments. This is mainly because the random magnetic anisotropy, which inevitably exists in real SG materials, is not introduced in our present model. Furthermore, in real SG magnets, spins do not necessarily sit on a simple-cubic lattice, nor interact with other spins via the nearest-neighbor $\pm J$ coupling, *etc.* In spite of these obvious limitations, it might be interesting to try to compare our present magnetic phase diagram with the experimental one for Heisenberg-like SG magnets. Chirality scenario claims that, in the high-field region where the anisotropy is negligible relative to the applied magnetic field, the SG transition line should essentially be given by the chiral-glass transition line of the fully isotropic system. If so, our present result entails that the SG transition line of real Heisenberg-like SG should be almost vertical against the temperature axis in the high-field regime where the magnetic field overwhelms the random magnetic anisotropy. In Fig.21(a), we reproduce the experimental H - T phase diagram of canonical SG AuFe from Ref. [11]. In the same figure, we also show our present result of the chiral-glass transition line, scaled in the following way. We try to mimic the real system by the classical Heisenberg Hamiltonian with an effective coupling J and an effective magnetic field H , which is defined in terms of Eq.(2). First, we estimate the zero-field transition temperature of the hypothetical *isotropic* system to be $T_g \approx 10\text{K}$, by extrapolating the high-field GT-like transition line of AuFe to $H = 0$. Then, with the knowledge of our present estimate of $T_{\text{CG}} \approx 0.2J$, we estimate the relevant J roughly to be 50K. The field intensity H is then translated into the field intensity in the standard unit H^* by the relation $H = p_{\text{eff}}H^*$, p_{eff} being the effective Bohr number: In case of AuFe, p_{eff} was experimentally estimated to be $4.55\mu_B$, where μ_B is the Bohr magneton [31]. Thus, our Fig.20 suggests that the SG phase boundary of AuFe might stay nearly vertical up to the field as high as $H \sim 10T_{\text{SG}}(0) \sim 40[\text{T}]$. Of course, considering the difference in microscopic details between the present model and real AuFe, one cannot expect a truly quantitative correspondence here. Anyway, further high-field experiments on AuFe and other Heisenberg-like SG magnets might be worthwhile to determine the SG phase boundary in the high-field regime.

In order to make further comparison with the experimental phase diagram in the low-field regime, it is essential to examine the effects of random magnetic anisotropy inherent to real SG materials. Indeed, in the low-field regime where the applied field intensity is comparable to or weaker than the random magnetic anisotropy, the chirality scenario predicts the appearance of a singular crossover line which has some character of the AT-line of the mean-field model [17,32]. In order to make further insight into the spin-glass and the chiral-glass orderings in magnetic fields and to check further the validity of the chirality scenario, it would be interesting to make similar finite-field simulations for the *anisotropic* 3D Heisenberg SG model.

ACKNOWLEDGEMENTS

The numerical calculation was performed on the HITACHI SR8000 at the supercomputer system, ISSP, University of Tokyo. The authors are thankful to Dr. K. Hukushima, Dr. H. Yoshino and Dr. I. A. Campbell for useful discussion.

- [1] For reviews on spin glasses, see *e. g.*, (a) K. Binder and A. P. Young: *Rev. Mod. Phys.* **58** (1986) 801; (b) K. H. Fischer and J. A. Hertz: *Spin Glasses* Cambridge University Press (1991); (c) J. A. Mydosh: *Spin Glasses* Taylor & Francis (1993); (d) A. P. Young (*ed.*): *Spin glasses and random fields* World Scientific, Singapore (1997).
- [2] J. A. Olive, A. P. Young and D. Sherrington: *Phys. Rev.* **B34** (1986) 6341.
- [3] F. Matsubara, T. Iyota and S. Inawashiro: *Phys. Rev. Lett.* **67** (1991) 1458.
- [4] H. Kawamura: *Phys. Rev. Lett.* **68** (1992) 3785; *Int. J. Mod. Phys.* **C7** (1996) 6341.
- [5] H. Yoshino and H. Takayama: *Europhys. Lett.* **22** (1993) 631.
- [6] H. Kawamura: *J. Phys. Soc. Jpn.* **64** (1995) 26.
- [7] H. Kawamura: *Phys. Rev. Lett.* **80** (1998) 5421.
- [8] K. Hukushima and H. Kawamura: *Phys. Rev.* **E61** (2000) R1008.
- [9] F. Matsubara, S. Endoh and T. Shirakura: *J. Phys. Soc. Jpn.* **69** (2000) 1927.
- [10] G. G. Kenning, D. Chu and R. Orbach: *Phys. Rev. Lett.* **66** (1991) 2923.
- [11] D. Petit, L. Fruchter, and I. A. Campbell: *Phys. Rev. Lett.* **83** (1999) 5130.
- [12] D. Sherrington and S. Kirkpatrick: *Phys. Rev. Lett.* **35** (1975) 1792. S. Kirkpatrick and D. Sherrington: *Phys. Rev.* **B17** (1978) 4384.
- [13] G. Kotliar and H. Sompolinsky: *Phys. Rev. Lett.* **53** (1984) 1751.
- [14] J. R. L. de Almeida and D. J. Thouless: *J. Phys.* **A11** (1978) 983.
- [15] M. Gabay and G. Toulouse: *Phys. Rev. Lett.* **47** (1981) 201.
- [16] H. Kawamura and S. Miyashita: *J. Phys. Soc. Jpn.* **53** (1985) 4138.
- [17] H. Kawamura and D. Imagawa: *cond-mat/0106097*.
- [18] K. Hukushima and K. Nemoto: *J. Phys. Soc. Jpn.* **65** (1995) 1604.
- [19] E. Marinari, C. Naitza, F. Zuliani, G. Parisi, M. Picco and F. Ritort: *Phys. Rev. Lett.* **81** (1998) 1698.
- [20] H. Bokil, A.J. Bray, B. Drossel and M.A. Moore: *Phys. Rev. Lett.* **82** (1999) 5174.
- [21] E. Marinari, C. Naitza, F. Zuliani, G. Parisi, M. Picco and F. Ritort: *Phys. Rev. Lett.* **82** (1999) 5175.
- [22] G. Parisi, M. Picco and F. Ritort: *Phys. Rev.* **E60** (1999) 58.
- [23] K. Hukushima and H. Kawamura: *Phys. Rev.* **E62** (2000) 3360.
- [24] F. Ritort and M. Sales: *cond-mat/0003336*.
- [25] M. Picco, F. Ritort and M. Sales: *cond-mat/0009292*.
- [26] H. Kawamura and M.S. Li: *cond-mat/0106551*.
- [27] For the static critical exponents, see, for example, (a) N. Kawashima and A. P. Young: *Phys. Rev.* **B53** (1996), 484; (b) E. Marinari, G. Parisi and J. J. Ruiz-Lorenzo: *Phys. Rev.* **B58** (1998) 14852; (c) B. A. Berg and W. Janke: *Phys. Rev. Lett.* **80** (1998) 4771; (d) M. Palassini and S. Caracciolo: *Phys. Rev. Lett.* **82** (1999) 5128; (e) H.G. Ballesteros, A. Cruz, L.A. Fernández, V. Martín-Mayor, J.J. Ruiz-Lorenzo, A. Tarancón, P. Téllez, C.L. Ulod and C. Ungil: *Phys. Rev.* **B62** (2000) 14237.
- [28] For the dynamical critical exponents, see, for example, (a) A. T. Ogielski: *Phys. Rev.* **B32**(1985) 7384.; (b) L. W. Bernardi, S. Prakash and I. A. Campbell: *Phys. Rev. Lett.* **77**(1996) 2798.
- [29] See, for example, (a) N. de Cortenay, H. Bouchiat, H. Hurdequite and A. Fert: *J. Physique* **47**(1986) 2659; (b) H. Bouchiat: *J. Physique* **47**(1986) 71; (c) L. P. Lévy and A. T. Ogielski: *Phys. Rev. Lett.* **57**(1986) 3288.
- [30] K. Hukushima and H. Kawamura: unpublished.
- [31] A. F. J. Morgownik and J. A. Mydosh: *Solid. State. Comm.* **47**(1983) 321.
- [32] H. Kawamura: unpublished.